Journal of Nuclear Medicine, published on October 20, 2016 as doi:10.2967/jnumed.114.151878

Brain FDG-PET metabolic abnormalities in patients with long-lasting macrophagic myofasciitis

Running foot line: Brain FDG-PET in patients with MMF

Authors:

Axel Van Der Gucht[1]; Mehdi Aoun Sebaiti[2,3], Eric Guedj[4]; Jessie Aouizerate[3,5,6]; Sabrina Yara[3], Romain K. Gherardi[3,5,6]; Eva Evangelista[1]; Julia Chalaye[1]; Anne-Ségolène Cottereau[1]; Antoine Verger[7]; Anne-Catherine Bachoud-Levi[2,8]; Emmanuel Itti[1]; François-Jérôme Authier[3,5,6]

Affiliations:

[1]Department of Nuclear Medicine, H. Mondor Hospital, Assistance Publique-Hôpitaux de Paris/Paris-Est University, Créteil, France

[2]Deparment of Neurology, H. Mondor Hospital, Assistance Publique-Hôpitaux de Paris/Paris-Est University, Créteil, France;

[3]INSERM U955-Team 10, Créteil, France

[4]Department of Nuclear Medicine, CHU La Timone, Assistance Publique-Hôpitaux de Marseille, Marseille, France;

[5]Department of Pathology, H. Mondor Hospital, Assistance Publique-Hôpitaux de Paris/Paris-Est University, Créteil, France;

[6]Reference Center for Neuromuscular Disorders, H. Mondor Hospital, Assistance Publique-Hôpitaux de Paris, Créteil, France;

[7]CHU Nancy, Nuclear Medecine & Nancyclotep Experimental Imaging Platform, Nancy, France;

[8]INSERM U955-Team 1, Créteil, France.

Corresponding author

Axel Van Der Gucht, MD

Department of Nuclear Medicine. Hôpital Henri Mondor AP-HP, Paris-Est University

51 Ave. du Mal de Lattre de Tassigny, F-94010 Créteil, France

Phone (+33)149812790/Fax (+33)149812794

E-mail:axel.vandergucht@gmail.com

ABSTRACT

Purpose: Aim of this study was to characterize brain metabolic abnormalities in patients with macrophagic myofasciitis (MMF), and the relation with cognitive dysfunction using Positron emission tomography with ^{18}F-fluorodeoxyglucose (FDG-PET).

Methods: FDG-PET brain imaging and a comprehensive battery of neuropsychological tests were performed in 100 consecutive MMF patients (mean age 45.9±12 y; women, 74%). Images were analyzed using statistical parametric mapping (SPM12). Using analysis of covariance, all FDG-PET brain images of MMF patients were compared to a reference population of 44 healthy subjects matched for age (mean age 45.4±16 y; p=0.87) and gender (women, 73%; p=0.88). The neuropsychological assessment identified four categories of patients with: no significant cognitive impairment (n=42); frontal sub-cortical (FSC) dysfunction (n=29); papezian dysfunction (n=22); and callosal disconnection (n=7).

Results: In comparison with healthy subjects, analysis of covariance of the whole population of patients with MMF exhibited a spatial pattern of cerebral glucose hypometabolism ($p<0.001$) involving occipital lobes, temporal lobes, limbic system, cerebellum and frontoparietal cortices. The subgroup of patients with FSC dysfunction exhibited larger extents of involved area (35223 voxels vs. 13680 voxels in the subgroup with papezian dysfunction and 5453 voxels in patients without cognitive

impairment). Not significant result was obtained in the last subgroup due to its small population size.

Conclusion: Our study identified in MMF patients a peculiar spatial pattern of a cerebral glucose hypometabolism mostly marked in MMF patients with FSC dysfunction. Further studies are needed to determine wether this pattern could represent a diagnostic biomarker of MMF in patients with chronic fatigue syndrome and cognitive dysfunction.

INTRODUCTION

Macrophagic myofasciitis (MMF) is an emerging condition with highly specific myopathological alterations found at deltoid muscle biopsy witnessing the abnormal long-term persistence of aluminum hydroxide adjuvant particles at the site of previous intramuscular injections of aluminium hydroxide-containing vaccines including hepatitis B, hepatitis A and most tetanus toxoid (*1,2*). MMF belongs to rare diseases (#ORPHA592, ICD-10 #M60.8, http://www.orpha.net/) and its prevalence is not exactly known. In most patients the typical clinical manifestations associated with MMF include arthromyalgias and chronic fatigue, occurring several months or years after the last vaccine injection (*3–5*) and cognitive impairment (*6*). The MMF-associated cognitive dysfunction has been neglected for a long time and was incorrectly considered as non-specific. Indeed, chronic pain, chronic fatigue states, and depressive syndromes are known to impair intellectual or cognitive performance. The prevalence of cognitive complaints ranged from 20 to 68% (*3,6–9*). The MMF-associated cognitive dysfunction resembles that observed upon chronic exposure to aluminum particles and in patients infected by hepatitis C virus or human immunodeficiency virus (HIV) (*6*). At follow-up, it appears stable over time, both in structure and severity (*10*). The neuropsychological profile of the MMF-associated cognitive dysfunction suggests underlying cortico-subcortical brain lesions, possibly of inflammatory or toxic origin. Experimental data evidenced that after parenteral injections of aluminum hydroxide, aluminum

particles can translocate into the brain tissue where they remain trapped (*11–14*). However, to our knowledge, there is no pathological evidence for brain damages specifically associated with MMF (*7*). In a recent perfusion single-photon emission computed tomography study of 76 MMF patients with varying degrees of cognitive impairment, we have shown a positive correlation between neuropsychological scores and brain perfusion in the posterior associative cortex, including cuneus, precuneus, occipital lingual areas, the periventricular white matter/corpus callosum, and the cerebellum, while negative correlation was found with amygdalo-hippocampal/entorhinal complexes (*15*). Also, a significant decreased uptake of FDG in a symmetrical pattern involving occipital lobes, temporal lobes and cerebellum was recently described during the diagnostic work-up of marked cognitive impairment, diffuse myalgias and sensory/visual disorders in a 44 y-old woman with histopathological features of MMF at deltoid muscle biopsy (*16*).

Purpose of the present study was to investigate brain glucose metabolism in a large series of MMF patients with varying degrees of neurospychological alteration, in order to disclose a cerebral glucose metabolism pattern compared with normal controls.

MATERIALS AND METHODS

Patients

The study population included consecutive symptomatic patients with histopathological features of MMF at muscle biopsy. Patients with a

history of cerebral disease, psychiatric disease, depressive symptoms and psychotropic medication were excluded. All patients underwent both FDG-PET/CT brain and neuropsychological testing (which are routinely performed in our center) as standard care and the Institutional Review Board (IRB, Comité de Protection des Personnes Ile-de-France VI) took into account the retrospective nature of this study approved the protocol (December 18, 2013) and waived the need for patient informed consent.

Control group

Healthy controls from the NCT00484523 clinical trial, matched for age and gender, were included. They were free from neurological/psychiatric disease and cognitive complaints, had a normal brain MRI and underwent a PET scan prior to a standardized neurological examination including a Mini Mental State Examination to check the lack of cognitive disorder.

Neuropsychological assessment

MMF patients underwent a comprehensive battery of neuropsychological tests exploring specific domains of the MMF-associated cognitive disorder (Table 1). Assessment of executive functions included tests exploring, working memory (backward digit span and Zazzo cancellation tests), flexibility (Trail Making Test, TMT), inhibition (Stroop test), and planning (Rey-Osterrieth test). Attention was explored by the Zazzo cancellation tests too. Long-term visual memory

was assessed by the Rey-Osterrieth delayed recall. Immediate verbal memory was assessed using the forward digit span, and episodic verbal memory Grober & Buschke long-term free (recovery capacity) and cued (storage capacity) recall. Finally, interhemispheric connection was tested by dichotic listening of words and sentences tasks, successively.

Apart from the evaluation of the dichotic listening where raw performance scores were expressed as a mean number of words/sentences compared to controls, all others raw performance scores were converted into mean Z-scores by comparison with a control population in order to express pathological threshold at -1.65 standard deviation of the normal average, as previously described *(6)*. Therefore, apart from the results of TMT and Stroop Interference (expressed as a time) where a mean Z-score < or $\geq$ 0 respectively indicated a good and a poor performance, for all others tests, a mean Z-score or a mean number of words/sentences $\geq$ 0 indicated good performance, while a mean Z-score or a mean number of words/sentences < 0 indicated poor performance.

At the end of neuropsychological assessment, patients were classified into four general categories: (i) no significant cognitive impairment; (ii) FSC dysfunction; (iii) papezian dysfunction; and (iv) callosal disconnection. Patients considered as cognitively healthy, were those who performed over the pathological threshold on all tests (1.65 standard deviation). Patients included in the group with FSC dysfunction

were those who had pathological performances on executive functions' tests (TMT, backward digit span, free recall of Grober and Buschke's test, Rey-Osterrieth figure type of copy, Zazzo's cancellation test, Stroop test and verbal fluency). They obtained good performances on episodic memory and dichotic listening tests. Patients identified with papezian dysfunction had similar executive dysfunction as group (ii), but demonstrated worse performances on episodic memory test. They showed pathological results on the three total recall tasks and the delayed total recall of Grober and Buschke's test, which assesses storage and consolidation capacities. Finally, patients with callosal disconnection potentially had the same cognitive troubles than patients included in the two previous groups. They had the particularity to obtain pathological results on the dichotic listening test which showed left ear extinction, and therefore, a callosal disconnection.

FDG-PET/CT acquisition

Brain imaging of MMF patients was performed on a Gemini GXL PET/CT camera (Philips, Da Best, The Netherlands) after intravenous injection of 2 MBq/kg ^{18}F-FDG. Patients were required to fast for at least 6 h before undergoing the scan, had normal blood glucose levels and were maintained in neurosensory resting 10 min before and for 30 min after injection. A low-dose helical CT was then performed for anatomical correlation and attenuation correction (X-ray tube tension of 120 kV, current of 80-100 mAs, rotation time 0.5 s, pitch 0.938, and slice

thickness 2 mm), followed by a 1-step emission scan of 15 min duration. Images were reconstructed using a line of response-row action maximum likelihood algorithm (2 iterations, 28 subsets, postfilter 5.1 mm), with CT attenuation correction (matrix size of 128x128, voxel size 2x2x2 mm^3). Brain imaging of healthy controls had previously been performed on a Discovery ST PET/CT camera (General Electric, Milwaukee, WI), using similar acquisition parameters (1 step of 15 min, 30 min after intravenous injection of 150 MBq ^{18}F-FDG) but slightly different reconstruction algorithm, i.e. ordered subset expectation maximization (5 iterations, 32 subsets), with CT attenuation correction, in 256x256 matrix and 0.8x0.8x0.8 mm^3 voxel size.

Statistical parametric mapping analysis

All FDG-PET brain image volumes were spatially normalized onto the Montreal Neurological Institute template (McGill University, Montreal, Canada) using a 12-parameter affine transformation, followed by non-linear transformations. Dimensions of the resulting voxels were 2x2x2 mm^3. Images were smoothed using a Gaussian filter (FWHM 10 mm) to blur individual variations in anatomy and to increase the signal-to-noise ratio. Spatial preprocessing and statistical analysis were performed using the statistical parametric mapping (SMP12) software implemented in Matlab version R2014a (Mathworks Inc., Sherborn, MA). Using analysis of covariance, cerebral FDG-PET images of all patients and

images of each subgroup were compared with images from the control group in order to identify a “MMF glucose metabolism pattern”. Results were collected at a P-value<0.005 at the voxel level, for clusters k≥200 voxels (corrected for cluster volume) with adjustment for age and gender, these nuisance variables being known to have influence on regional brain metabolism. All significant results were listed with the individual k-value, which represents the number of significant voxels in the particular cluster (cluster size), brain regions, side of the hemisphere, Brodmann areas involved and the peak T-value (defined through our statistical model as standard deviation of measure of cerebral glucose metabolism in comparison to the reference population).

Statistical analysis

Quantitative variables were expressed as the mean and standard deviation. Categorical variables were expressed as a percentage. Inter-group comparisons were performed with *t* test. For each test, P-values<0.05 were considered statistically significant.

RESULTS

Clinical features

The group with MMF consisted of 100 patients (women, 74%), included between 2012 and 2015. These patients were aged 16-65 years (mean age 45.9±12 years) with a mean socio-cultural level (years of education

after high school) of 5.6±1.3 y. Chronic myalgias, fatigue and cognitive disorders were found in 94 (94%), 69 (69%) and 76 (76%) patients, respectively. The mean delay between FDG-PET brain and neuropsychological evaluation was 0.81±1.9 months. Patient performances on neuropsychological tests are displayed in Table 1 (whole population and after separation in four neurosychological categories).

Group (i) patients (n=42; 42%) did not have any pathological results on cognitive tests. Patients included in the second category (FSC) (n=29; 29%) obtained Z-scores higher/lower than 1.65/-1.65 standard deviation on the Stroop test (mean of interference-denomination scores was 1.7±1.3), the TMT (mean of TMT B–TMT A scores was 1.3±1.7) and the 3 signs' condition of Zazzo's cancellation test (mean was -1.8±0.8). Group (iii) patients (n=22; 22%) demonstrated poor performance on the three cued recall tests (Total Recall [TR]1 = -1.1±1.5; TR2 = -1.7±3.4; TR3 = -2.1±4.6) and the delayed cued recall (mean was -11.4±14.2) of the Grober-Buschke test. It should be noted that they obtained good results on the delayed recall of the Rey Osterrieth figure (mean was -0.6±0.9). In addition, they were also bad performers on the Stroop test (mean of interference-denomination scores was 1.3±2) and the 3 signs' condition of Zazzo's cancellation test (mean was -1.6±1.4). Finally, patients with callosal disconnection (n=7; 7%) presented pathological performances especially for the left ear words and sentences' condition

on the dichotic listening test (means were respectively -14.9±15.2 for the words' condition and -6.7±6 for the sentences' condition). They were also deficient on the Stroop test (means was 2.1±2.2 for interference-denomination scores and 2.2±4.8 for the number of errors at the interference-denomination scores), the TMT (mean of TMT B–TMT A scores was 2.8±2.9) and the 3 signs' condition of Zazzo's cancellation test (mean was -1.8±1).

The selected control population consisted of 44 healthy subjects similar for age (mean age 45.4±16, p=0.87) and gender (women, 73%; p=0.88) with the whole-group of patients.

MMF-associated brain metabolism changes

As illustrated in Figure 1, analysis of covariance analysis between 93 patients with MMF (groups i, ii, and iii) and the control group exhibited a symmetrical pattern of hypometabolism involving the occipital lobes, temporal lobes, limbic system, anterior and posterior lobes of the cerebellum and frontoparietal cortices (sum, 6354 voxels; $p<0.001$, Table 2).

The statistical parametric mapping analysis by subgroup showed that patients with FSC dysfunction (ii) exhibited the largest extent of involved area, 35223 voxels vs. 13680 voxels for the group with papezian dysfunction (iii), and 5453 voxels in patients without cognitive impairment (i). Not significant result was obtained in the last subgroup

(iv) due to its small population size. Abnormalities are illustrated and listed in Figure 2 and Table 2 respectively.

DISCUSSION

The significant clusters revealed by statistical parametric mapping analysis in this large population of patients with varying severities of cognitive dysfunction provides a spatial pattern of cerebral glucose metabolism in patients with long-lasting aluminum hydroxide-induced MMF.

Hypometabolism of occipital cortex is consistent with visuospatial impairment found at neuropsychological assessment. Hypoperfusion of lingual occipital regions was found by statistical parametric mapping analysis with $P<0.001$ in our previous study with technetium-99m ethyl cysteinate dimer (^{99m}Tc-ECD) single-photon emission computed tomography (*15*), but was not apparent to the naked eye. Indeed, it is known that physiological ^{99m}Tc-ECD uptake is particularly marked in the visual cortex, compared to other perfusion tracers such as technetium-99m hexamethylpropylene amine oxime (^{99m}Tc-HMPAO) (*17*), thus making it difficult to identify hypoperfusions in these regions on routine image interpretation. With FDG-PET/CT, to the contrary, this spatial pattern of cerebral glucose hypometabolism is the predominant imaging feature in MMF patients with $P<0.001$ and can be easily diagnosed on routine interpretation (*16*). Probably for similar reasons of differing tracer uptake mechanisms, perfusion imaging with statistical parametric

mapping analysis was able to identify periventricular abnormalities in the subset of patients with callosal dysfunction, suggesting impairment of subcortical connection between cerebral hemispheres, while FDG imaging, which measures glucose consumption in the neuron bodies, was unable to identify dysfunction in the periventricular areas in patients with callosal dysfunction. Therefore, both techniques are complementary; in our center preliminary results using diffusion-tensor imaging have emphasized interruption of callosal pathways in these patients and it is expected that simultaneous diffusion-tensor imaging/FDG-PET imaging may help to assess MMF-associated cognitive disorder in a near future.

Cerebellum is known to be involved in motor functions. It has also an important role in cognitive processing, particularly in executive functions (*18*). This activity is due to the numerous connections between the cerebellum and cortical areas through the cortico-ponto-cerebellar pathways (*19*). Afferent fibers mostly come from associative parietal and occipital areas, which are significantly impaired in our study. Limbic system, including amygdalo-hippocampal/entorhinal complexes and cingulate gyrus, also play an essential role in long-term memory storage, and are involved in the Papez circuit (*20*). These structures are the first to be impaired in mild cognitive impairment conversion into Alzheimer's disease (*21*). This pattern has been described recently at the individual level (16) in FDG-PET/CT and on a population level using perfusion SPECT technique (*15*). FDG-PET/CT appears more sensitive

than perfusion SPECT to detect posterior cortical and subcortical abnormalities in this setting.

Concerning the neuropsychological profile, all patients with significant cognitive impairment (groups ii, iii and iv) displayed a marked deficit of executive functions notably affecting inhibition, flexibility and working memory, with also difficulties in selective attention. Executive difficulties were associated with papezian dysfunction (group iii) and callosal disconnection (group iv). In group iii, amnesic trouble especially concerned the storage and the consolidation abilities in verbal episodic memory. It should be noted that they correctly performed in visuo-spatial modality. Interestingly, in patients without significant cognitive dysfunctioning (group i) FDG-PET showed brain hypometabolism, with a spatial pattern similar to that observed in groups ii and iii patients, but less intense, that could represent a presymptomatic state. Long-term follow-up will be needed to determine whether FDG-PET hypometabolism could be predictive of cognitive dysfunctioning.

Lastly, several SPECT perfusion (*22–24*) and FDG-PET studies have investigated cerebral changes induced by fibromyalgia and reported divergent results. Whereas Yunus et al. found no abnormalities of FDG uptake between 12 patients with fibromyalgia and 7 healthy subjects (*25*), Walitt et al. described in a pilot study an increase in limbic metabolism with concomitant symptomatic improvement in 9 patients with fibromyalgia (*26*). Results also are unclear about cerebral changes associated with chronic fatigue syndrome. In 26 patients with chronic

fatigue syndrome, Siessmeier et al. showed that the cingulate gyrus and adjacent mesial cortex were involved bilaterally in most patients (*27*). A significant hypometabolism in right mediofrontal cortex and brainstem was described by Tirelli et al. in 18 patients with chronic fatigue syndrome (*28*). Then, it will be very interesting in further study, to use as control group, patients with fibromyalgia or patients with chronic fatigue syndrome in order to eliminate any cerebral metabolic changes associated with the painful or fatigue sensation.

CONCLUSION

The current study identified a peculiar spatial pattern of cerebral glucose hypometabolism in patients with long-lasting aluminum hydroxide-induced MMF. It appeared mostly marked in MMF patients with FSC dysfunction. Further studies are needed to determine wether this pattern could represent a diagnostic biomarker of MMF in patients with chronic fatigue syndrome and cognitive dysfunction.

ACKNOWLEDGMENTS

This work was supported by grants from Région Ile-de-France through "Partenariats institutions-citoyens pour la recherche et l'innovation" (PICRI programs 2010 and 2014).

This work has been carried out thanks to the support of the A*MIDEX project (n° ANR-11-IDEX-0001-02) funded by the « Investissements

d’Avenir » French Government program, managed by the French National Research Agency (ANR)

REFERENCES

1. Gherardi RK, Coquet M, Chérin P, et al. Macrophagic myofasciitis: an emerging entity. Groupe d'études et recherche sur les maladies musculaires acquises et dysimmunitaires (GERMMAD) de l'association française contre les myopathies (AFM). *Lancet*. 1998 1;352:347–352.

2. Gherardi RK, Coquet M, Cherin P, et al. Macrophagic myofasciitis lesions assess long-term persistence of vaccine-derived aluminium hydroxide in muscle. *Brain*. 2001;124:1821–1831.

3. Authier F-J, Sauvat S, Champey J, Drogou I, Coquet M, Gherardi RK. Chronic fatigue syndrome in patients with macrophagic myofasciitis. *Arthritis Rheum*. 2003;48:569–570.

4. Santiago T, Rebelo O, Negrão L, Matos A. Macrophagic myofasciitis and vaccination: consequence or coincidence? *Rheumatol Int*. 2014;35:189-192.

5. Rigolet M, Aouizerate J, Couette M, et al. Clinical features in patients with long-lasting macrophagic myofasciitis. *Neurodegeneration*. 2014;5:230.

6. Couette M, Boisse M-F, Maison P, et al. Long-term persistence of

vaccine-derived aluminum hydroxide is associated with chronic cognitive dysfunction. *J Inorg Biochem*. 2009;103:1571–1578.

7. Gherardi RK, Authier F-J. Aluminum inclusion macrophagic myofasciitis: a recently identified condition. *Immunol Allergy Clin North Am*. 2003;23:699–712.

8. Guis S, Mattei JP, Nicoli F, et al. Identical twins with macrophagic myofasciitis: genetic susceptibility and triggering by aluminic vaccine adjuvants? *Arthritis Rheum*. 2002;47:543–545.

9. Guis S, Pellissier J-F, Nicoli F, et al. HLA-DRB1*01 and macrophagic myofasciitis. *Arthritis Rheum*. 2002;46:2535–2537.

10. Passeri E, Villa C, Couette M, et al. Long-term follow-up of cognitive dysfunction in patients with aluminum hydroxide-induced macrophagic myofasciitis (MMF). *J Inorg Biochem*. 2011;105:1457–1463.

11. Wen GY, Wisniewski HM. Histochemical localization of aluminum in the rabbit CNS. *Acta Neuropathol*. 1985;68:175–184.

12. Redhead K, Quinlan GJ, Das RG, Gutteridge JM. Aluminium-adjuvanted vaccines transiently increase aluminium levels in murine

brain tissue. *Pharmacol Toxicol*. 1992;70:278–280.

13. Sahin G, Varol I, Temizer A, Benli K, Demirdamar R, Duru S. Determination of aluminum levels in the kidney, liver, and brain of mice treated with aluminum hydroxide. *Biol Trace Elem Res*. 1994;41:129–135.

14. Khan Z, Combadière C, Authier F-J, et al. Slow CCL2-dependent translocation of biopersistent particles from muscle to brain. *BMC Med*. 2013;11:99.

15. Van Der Gucht A, Aoun Sebaiti M, Itti E, et al. Neuropsychological correlates of brain perfusion SPECT in patients with macrophagic myofasciitis. *PloS One*. 2015;10:e0128353.

16. Van Der Gucht A, Aoun-Sebaiti M, Kauv P, et al. FDG-PET/CT Brain findings in a patient with macrophagic myofasciitis. *Nucl Med Mol Imaging*. 2016;50:80-84.

17. Hyun Y, Lee JS, Rha JH, Lee IK, Ha CK, Lee DS. Different uptake of 99mTc-ECD and 99mTc-HMPAO in the same brains: analysis by statistical parametric mapping. *Eur J Nucl Med*. 2001;28:191–197.

18. Schmahmann JD. Disorders of the cerebellum: ataxia, dysmetria

of thought, and the cerebellar cognitive affective syndrome. *J Neuropsychiatry Clin Neurosci*. 2004;16:367–378.

19. Schmahmann JD, Doyon J, McDonald D, et al. Three-dimensional MRI atlas of the human cerebellum in proportional stereotaxic space. *NeuroImage*. 1999;10:233–260.

20. Eichenbaum H. A cortical-hippocampal system for declarative memory. *Nat Rev Neurosci*. 2000;1:41–50.

21. Drzezga A, Lautenschlager N, Siebner H, et al. Cerebral metabolic changes accompanying conversion of mild cognitive impairment into Alzheimer's disease: a PET follow-up study. *Eur J Nucl Med Mol Imaging*. 2003;30:1104–1113.

22. Kwiatek R, Barnden L, Tedman R, et al. Regional cerebral blood flow in fibromyalgia: single-photon-emission computed tomography evidence of reduction in the pontine tegmentum and thalami. *Arthritis Rheum*. 2000;43:2823–2833.

23. Gur A, Karakoc M, Erdogan S, Nas K, Cevik R, Sarac AJ. Regional cerebral blood flow and cytokines in young females with fibromyalgia. *Clin Exp Rheumatol*. 2002;20:753–760.

24. Guedj E, Cammilleri S, Niboyet J, et al. Clinical correlate of brain

SPECT perfusion abnormalities in fibromyalgia. *J Nucl Med*. 2008;49:1798–1803.

25. Yunus MB, Young CS, Saeed SA, Mountz JM, Aldag JC. Positron emission tomography in patients with fibromyalgia syndrome and healthy controls. *Arthritis Rheum*. 2004;51:513–518.

26. Walitt B, Roebuck-Spencer T, Esposito G, et al. The effects of multidisciplinary therapy on positron emission tomography of the brain in fibromyalgia: a pilot study. *Rheumatol Int*. 2007;27:1019–1024.

27. Siessmeier T, Nix WA, Hardt J, Schreckenberger M, Egle UT, Bartenstein P. Observer independent analysis of cerebral glucose metabolism in patients with chronic fatigue syndrome. *J Neurol Neurosurg Psychiatry*. 2003;74:922–928.

28. Tirelli U, Chierichetti F, Tavio M, et al. Brain positron emission tomography (PET) in chronic fatigue syndrome: preliminary data. *Am J Med*. 1998;105:54S – 58S.

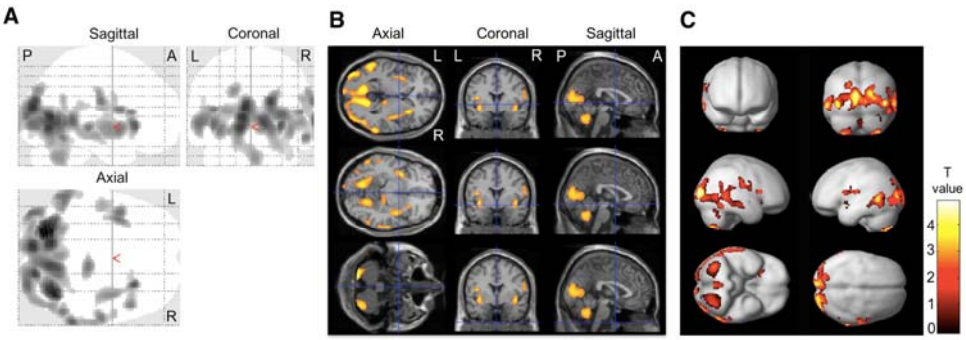

FIGURE 1. Significant hypometabolic brain regions of the whole population of patients (n=100) with MMF compared to scans from healthy subjects after adjustment for age and gender confirming a significant decreased uptake of FDG in a symmetrical spatial pattern of cerebral glucose metabolism involving the occipital cortex, temporal lobes, limbic system and cerebellum. Abnormalities are displayed with T-*score* value on 2-dimensional "Glass-brain" projection-images (A), slices of MRI template in axial, coronal and sagittal orientations (B) and projected onto a brain rendered 3D-MIP (C). P-value<0.005 at the voxel level for clusters k≥200 contiguous voxels (corrected for cluster volume). A, anterior; P, posterior; L, left; R, right.

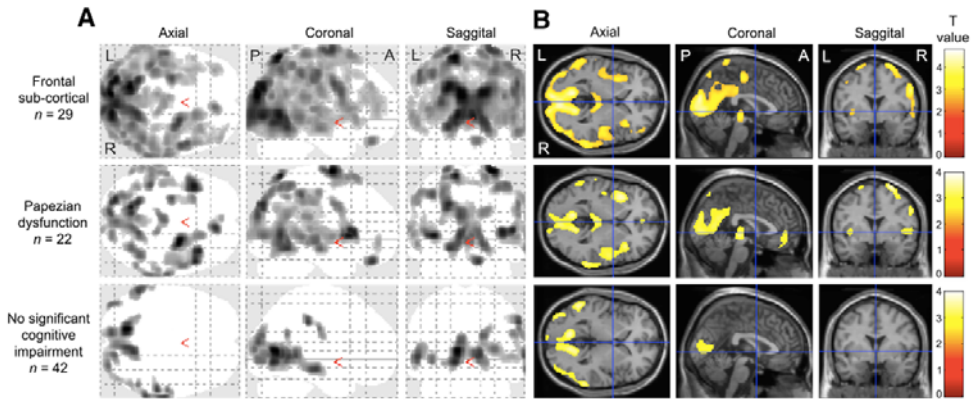

FIGURE 2. Significant hypometabolic brain regions by categories of patients with MMF (from the most severe spatial pattern to the less severe). Abnormalities are displayed with T-*score* value on 2-dimensional "Glass-brain" projection-images (A) and slices of MRI template in axial, coronal and sagittal orientations (B). P-value<0.005 at the voxel level for clusters k≥200 contiguous voxels (corrected for cluster volume). A, anterior; P, posterior; L, left; R, right.

Table 1. Neuropsychological assessment.

Characteristics		All patients		(i) No significant cognitive impairment (*n*=42)		(ii) Frontal sub-cortical dysfunction (*n*=29)		(iii) Papezian dysfunction (*n*=22)		(iv) Callosal disconnection (*n*=7)	
	n	Raw scores	Scores	Raw scores	Scores	Raw scores	Scores	Raw scores	Scores	Raw scores	Scores
Executive functions											
Stroop											
Color*	95	75.1±22.8	1.4±2.4	65.1±11.9	0.4±1	75.3±14.7	1.6±1.5	84.4±32.7	2.4±3.3	105.8±31.1	4±3.4
Word*	95	55.8±20.3	2±3.4	48.1±10	0.7±1.4	55.9±13.7	2.1±2.1	61.1±27.6	2.7±4.7	87±33.5	7.5±5.9
Interference*	95	142.2±49	1.4±2	115.9±23.4	0.2±0.8	155.1±31.9	2±1.1	158.6±69.4	2.1±2.8	194.3±73.1	3.8±3.1
Interference-Color*	95	67.2±33.3	1±1.6	50.7±19.2	0.1±0.9	79.8±27.6	1.7±1.3	74.2±43.4	1.3±2	88.5±50	2.1±2.2
Interference-Color Error*	95	0.5±1.3	1.4±2	0.5±1	0.2±1.2	0.4±1	0.2±1.2	0.3±0.8	0±1	1.8±3.6	2.2±4.8
Rey-Osterrieth											
Copy*	98	34.9±1.5	0±1	34.8±1.7	-0.1±1	35.1±1.2	0.1±0.7	35.1±1.5	0±1.2	34.9±1.7	0±1.3
Verbal memory											
Forward verbal digit span*	100	5.5±1	-0.7±0.9	5.6±0.7	-0.6±0.7	5.7±1	-0.6±0.9	5.4±1.3	-0.7±1.3	4.7±0.8	-1.4±0.8
Backward verbal digit span*	100	4.1±1.2	-0.7±1.2	4.6±1.2	-0.2±0.9	3.9±1	-0.9±1.2	3.7±1.1	-1.2±1.5	3.4±0.5	-1.3±0.8
Forward spatial digit span*	100	5.2±0.8	-0.9±0.8	5.4±0.8	-0.8±0.8	5.2±0.8	-1±0.9	5±0.8	-1.1±0.7	4.7±1.1	-1.4±1.1
Backward spatial digit span*	100	4.6±0.9	-0.1±1	4.8±0.9	0.1±0.9	4.6±0.9	-0.1±1	4.6±0.9	-0.2±1	4.1±0.7	-0.6±0.9
Memory functions											
Grober & Buschke											
IR*	100	15.2±1.2	-0.5±1.6	15.3±1.2	-0.4±1.5	15.6±0.8	-0.1±1.3	14.7±1.4	-1.2±1.7	14.9±1.7	-0.9±2.1
3FR*	100	30.9±6	-0.6±1.2	33.6±4.9	0±0.8	32±4.6	-0.5±1.1	25.3±5.5	-1.9±1.3	28±5.6	-1.1±1.2
TR1*	100	15±1.6	0.01±1	15.5±0.9	0.4±0.5	15.6±0.6	0.4±0.4	13.3±2.4	-1.1±1.5	14.6±1.3	-0.2±0.8
TR2*	100	15.3±1.5	-0.2±1.9	15.7±0.6	0.3±0.6	15.8±0.5	0.4±0.5	14.1±2.7	-1.7±3.4	15±0.8	-0.5±0.9
TR3*	100	15.6±1.2	-0.3±2.4	16±0.2	0.3±0.4	15.9±0.3	0.3±0.3	14.6±2.3	-2.1±4.6	15.3±0.8	-0.8±1.2
3TR*	100	45.9±4.1	1.9±4.1	47.1±1.2	3.1±1.2	47.3±1	3.3±1	41.9±7.1	-2.1±7.1	44.9±2.7	0.9±2.7
Rec*	100	15.6±1.2	-0.4±2	16±0.3	0.3±0.4	15.8±0.5	0.1±0.8	14.6±2.1	-2±3.5	15.3±1.5	-0.9±2.6
D-FR*	100	11.6±2.9	-0.9±1.7	13±2.1	-0.1±0.8	12.4±1.9	-0.5±1	8.1±2.6	-3±1.7	10.4±2.3	-1.5±1.6
D-TR*	100	15.2±1.9	-2.4±8.2	15.9±0.3	0.3±0.3	15.9±0.3	0.4±0.4	12.8±2.8	-11.4±14.2	15.1±1.2	-2.2±4.1
Visual memory											
Rey-Osterrieth Delayed recall*	98	20.3±5.8	-0.3±1	21.5±5.5	-0.1±0.9	20.5±5.4	-0.2±1.1	18.9±6.7	-0.6±0.9	16.7±4.4	-0.9±0.6
Verbal Fluency											
P letter*	99	18.8±7.2	-0.7±1.2	21.7±7.9	-0.2±1.4	17.9±5.6	-0.9±0.9	15.6±6.3	-1.1±1.1	15.6±4.7	-1.4±0.8
Animals*	99	28.8±8.9	-0.6±1.2	31.3±9.3	-0.1±1.3	28.6±7.6	-0.7±0.9	27±8.8	-0.8±1.2	19.7±5.8	-1.8±0.8
DO80*	97	78.7±1.5	-0.3±1.4	78.9±1.5	-0.1±1.1	78.5±1.7	-0.6±1.7	79.1±1.2	0±0.9	77.6±1.5	-1.7±1.5
Flexibility											

TMT A*	97	38.5±16.1	0.1±1.2	31.7±11.8	-0.4±0.7	41.9±14.7	0.4±1.1	42.5±19.4	0.4±1.4	51.7±18.5	1.2±1.7
TMT B*	97	95.5±43	0.8±1.7	72.6±19.7	-0.2±0.8	111.7±42.4	1.4±1.7	103.2±43.9	0.9±1.4	150.1±61.8	3.1±2.8
TMT B–TMT A*	97	58±34.4	0.7±1.5	41±14.1	0±0.7	69.8±37.9	1.3±1.7	60.7±30.8	0.8±1	98.4±57.1	2.8±2.9
Dichotic listening											
Left ear words**	90	48.7±11.2	-0.4±11.2	51.2±11	2.2±10.7	49.5±9.8	0.6±9.8	48.4±8.9	-1.3±9.2	34.6±1.5	-14.9±15.2
Right ear words**	90	51.1±9.5	-0.8±9.3	52.4±10.3	0.7±9.9	51.4±8.1	-0.1±8.2	49.6±9.4	-3±9.7	47.4±11	-4.9±9.3
Left ear sentences**	90	14.5±6	1.3±6.4	15.3±3.6	2.3±3.4	16.3±8.2	3.5±9	13.2±3.2	-0.5±3.3	6.7±5.1	-6.7±6
Right ear sentences**	90	17.6±4.6	2.7±5.1	17.6±3.6	2.9±3.8	18.5±6.4	3.9±7.3	17±2.9	1.5±3.3	16±5.3	0.7±3.7
Attention											
Zazzo 1 sign*	100	49.2±15.5	-1±1.1	54.1±14.6	-0.7±1	45±9.4	-1.3±0.7	47.4±20	-1.2±1.4	42.4±19.2	-1.5±1.3
Zazzo 2 signs*	100	49.3±14.4	-1±1	54.6±14.3	-0.7±1	44.4±8.5	-1.3±0.6	47.9±17.6	-1.1±1.2	42±15.3	-1.5±1.1
Zazzo 3 signs*	100	35.7±13.4	-1.4±1.1	41.1±12.7	-0.9±1.1	30.8±9.5	-1.8±0.8	33.3±16.2	-1.6±1.4	30.7±11.9	-1.8±1

* scores expressed as mean Z-score (mean±standard deviation)

** scores expressed as mean number of words/sentences compared to controls

IR : Immediate Recall; FR : Free Recall; TR : Total Recall; Rec : Recognition; D-FR : Delayed-Free Recall; D-TR : Delayed-Total Recall; OR : Oral Denomination; Trail making test

Table 2. Brain areas with significant decreased uptake of FDG after comparison with control group. Results were collected at a P-value<0.005 at the voxel level, for clusters k≥200 voxels with adjustment for age and gender.

K	Brain areas	Side	Labels	Peak value coordinates (mm)			T-value	P-value
				x	*y*	*z*		
Whole-group (n=100)								
328	Cerebellum	L	CPL	-22	-72	-60	4.82	<0.001
284	Cerebellum	R	CPL	36	-66	-62	4.29	<0.001
3901	Occipital lobe, Limbic lobe, Cerebellum, Sub-lobar	L, R	BA18-BA19-BA30-BA17-BA23-BA31-BA7-CAL-CPL	-12	-70	6	4.06	<0.001
455	Temporal lobe, Parietal lobar	R	BA21-BA22-BA39-BA40	66	-46	4	3.56	<0.001
439	Temporal lobe, Occipital lobe	L	BA37-BA39-BA21-BA22-BA19	-56	-54	0	3.55	<0.001
207	Frontal lobe	L, R	BA11-BA47	-8	22	-32	3.51	<0.001
236	Sub-lobar, Temporal lobe	L	BA13-BA38	-36	4	-8	3.47	0.001
271	Occipital lobe	L	BA19-BA18	-42	-86	0	3.33	0.001
233	Sub-lobar, Temporal lobe	R	BA13-BA21	40	-2	-8	3.11	0.001
Frontal sub-cortical dysfunction (n=29)								
33436	Occipital lobe, Parietal lobe, Frontal lobe, Temporal lobe, Limbic lobe, Sub-lobar, Cerebellum	L, R	BA19-BA18-BA40-BA7-BA6-BA31-BA21-BA22-BA37-BA13-BA17-BA2-BA4-BA3-BA39-BA30-BA23-BA9-BA44-BA42-BA46-BA1-BA41-BA8-BA45-BA10-BA20-BA47-BA43-BA5-BA36-BA29-BA24-CAL-CPL	-14	-66	66	4.78	<0.001
251	Frontal lobe	R	BA11-BA47	10	40	-26	3.71	<0.001
681	Midbrain, Sub-lobar, Limbic lobe, Temporal lobe	L, R	BA27-BA30-BA35-BA28	4	-24	-6	3.39	0.001
256	Frontal lobe, Limbic lobe	L, R	BA6-BA31	-2	-18	56	3.32	0.001
349	Frontal lobe	L	BA10-BA9-BA46	-34	40	34	3.25	0.001
250	Parietal lobe	L, R	BA7-BA5	-8	-46	78	3.20	0.001
Papezian dysfunction (n=22)								
766	Frontal lobe	R	BA6-BA8	28	-4	72	3.98	<0.001
1084	Sub-lobar, Frontal lobe, Temporal lobe, Parietal lobe	L	BA13-BA44-BA41-BA47-BA22-BA45-BA6-BA43	-38	14	2	3.83	<0.001
6494	Occipital lobe, Parietal lobe, Limbic lobe, Cerebellum, Frontal lobe, Temporal lobe	L, R	BA19-BA18-BA40-BA7-BA31-BA30-BA17-BA23-BA2-BA3-BA37-BA1-BA4-BA29-BA22-BA36-CAL-CPL	-14	-64	68	3.80	<0.001
2411	Temporal lobe, Frontal lobe, Sub-lobar, Parietal lobe	R	BA22-BA13-BA21-BA44-BA6-BA45-BA9-BA47-BA41-BA40-BA39	40	18	6	3.78	<0.001
399	Frontal lobe, Limbic lobe	L, R	BA11-BA32-BA10-BA47	12	40	-26	3.64	<0.001
351	Frontal lobe	L	BA6	-24	-14	74	3.45	0.001
605	Midbrain, Limbic lobe	L, R	BA27-BA30-BA35	0	-24	-4	3.38	0.001
516	Parietal lobe	R	BA7-BA40	44	-52	58	3.38	0.001
567	Parietal lobe, Temporal lobe, Frontal lobe	R	BA40-BA2-BA1-BA42-BA3-BA22-BA43-BA4	68	-34	22	3.18	0.001
256	Temporal lobe, Occipital lobe	L	BA37-BA21-BA22-BA19	-58	-62	-8	3.14	0.001
231	Temporal lobe, Parietal lobe	L	BA42-BA22-BA40-BA41-BA21	-66	-30	10	3.11	0.001
No significant cognitive impairment (n=42)								
4325	Occipital lobe, Temporal lobe, Limbic lobe, Parietal lobe, Cerebellum	L, R	BA18-BA19-BA21-BA30-BA17-BA22-BA23-BA37-BA31-BA7-BA40-BA39-BA20-CAL	-12	-70	8	4.00	<0.001
583	Temporal lobe, Occipital lobe	L	BA39-BA21-BA22-BA37-BA19	-58	-54	0	3.59	<0.001
333	Parietal lobe, Frontal lobe	R	BA40-BA2-BA3-BA4-BA1-BA43	58	-32	40	3.55	<0.001
212	Occipital lobe	L	BA19-BA18	-42	-86	-4	3.34	0.001
Callosal disconnection (n=7)								
No significant voxels								

BA, brodmann area; CAL, cerebellum anterior lobe; CPL, cerebellum posterior lobe; L, left; R, right